An Efficient Analysis Method for Artificial Dielectric Layers With Vertical Metal Inclusions Based on a Full-Wave Spectral-Domain Approach

Van Katwijk, Alexander J.; Neto, Andrea; Cavallo, Daniele

DOI
10.1109/TAP.2025.3529189

Publication date
2025

Document Version
Final published version

Published in
IEEE Transactions on Antennas and Propagation

Communication

An Efficient Analysis Method for Artificial Dielectric Layers With Vertical Metal Inclusions Based on a Full-Wave Spectral-Domain Approach

Alexander J. van Katwijk, Andrea Neto, and Daniele Cavallo

***Abstract*— We present an efficient method to analyze a periodic pin-patch structure, consisting of two artificial dielectric layers (ADLs) connected by vertical metal pins. ADLs are made of square metal patches in a periodic lattice and have recently been used as superstrates in antennas and arrays to enhance the bandwidth and scanning range. ADLs form an anisotropic effective medium, thus enabling a large scanning volume without supporting surface waves. However, the anisotropy increases the cross-polarization (X-pol) of the antenna in the diagonal plane. This problem can be reduced by introducing vertical metal pins in the ADL superstrate to form the pin-patch structure. The analysis method is based on a spectral method of moments (MoMs) and uses entire-domain basis functions in a hybrid Cartesian and cylindrical representation to accurately model the currents on the structure and scattering parameters under general plane-wave incidence.**

***Index Terms*— Artificial dielectrics, cross-polarization (X-pol), entire-domain basis functions, method of moments (MoMs), periodic structures, spectral domain.**

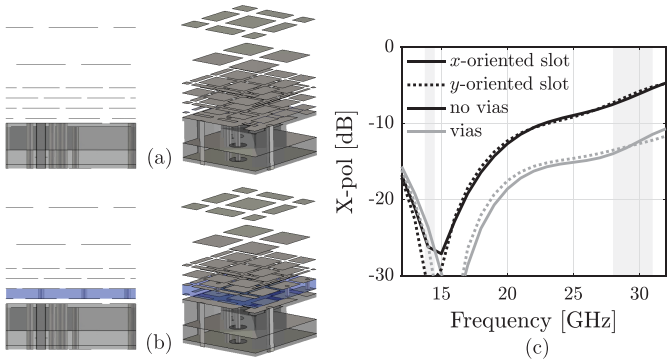

Fig. 1. Side and 3-D views of a connected array unit cell with ADLs (a) without and (b) with vertical pins. (c) X-pol for both unit cells when scanning to 60° in the diagonal plane.

I. Introduction

Wideband wide-scan arrays have gained increasing attention due to their ability to combine multiple functionalities in a single-antenna aperture. For many applications, a common requirement for these arrays is polarization agility. However, in the design process of these arrays, lower polarization purity is often accepted to achieve wider bandwidth and scanning range [1], [2].

In planar arrays, the ability to cover large bandwidths and wide-scan volumes is often achieved with dielectric or metal superstrates. One such planar array is the connected array [3], which can utilize a planar artificial dielectric consisting of square metal patches to increase the front-to-back ratio and improve the matching while scanning. The analysis of these artificial dielectric layers (ADLs) was previously studied in [4], where a closed-form solution for an equivalent layer reactance was defined. This type of artificial dielectric has anisotropic properties, where its effective refractive index decreases with the angle of propagation.

However, the ADL anisotropy also reduces the polarization purity when the array scans in the diagonal planes. This problem can be mitigated by reducing this anisotropy, as was described in [5]. A pin-patch structure was proposed, formed by connecting two layers of the ADL together using a vertical pin, similar to the geometry proposed by [6]. For example, [7] showed an array covering both the Ku- and Ka-transmit bands while scanning up to 60°. The designed unit cell is repeated in Fig. 1(a) and consists of six metal layers over a dual-polarized slot plane, which is placed over a dielectric substrate with a backing reflector. Its cross-polarization (X-pol) when it is scanned to 60° in the diagonal plane is shown in black in Fig. 1(c) to exceed −10 dB at higher frequencies. To show the effect of the pins on the X-pol, a dielectric slab with a relative permittivity of 2.2 and metal vias are added between the first two ADLs, as illustrated in Fig. 1(b). The X-pol of the new unit cell is shown in Fig. 1(c) to be reduced by about 5 dB over most of the band.

Since the structure has been proved to be effective, it is interesting to study pin-patch periodic elements independently to highlight their scattering properties. To this end, an efficient analysis method is desired. Homogenization techniques for the analysis of capacitively loaded wire medium were presented in [8], but they have limitations when wires are much shorter than the wavelength. Here, a full-wave approach is proposed, based on a spectral-domain method of moments (MoMs). Spectral-domain integral equation methods have been widely used for analyzing the scattering from periodic structures [9], [10]. Various methods for improved efficiency and accuracy of the solution have been proposed, for example, subdomains with nonconforming meshes [11] and mixed potential integral equations [12], [13]. Moreover, the choice of proper entire-domain basis functions can regularize the kernel of the integral equation (e.g., weighted Chebyshev polynomial in [14]) or reduce the number of unknowns [15].

The main novelty of this work is in the choice of a small set of suitable entire-domain basis functions that describe the physics of the problem, for efficient evaluation of the scattered field. We attempt to demonstrate that, for the specific structure under analysis (sub-wavelength pin-patch element), three types of basis functions are sufficient to describe the current on the structure for any plane-wave incidence. In the absence of pins, we postulate that two main modes are supported by a periodic layer of small patches: linear currents on the patches for transverse magnetic (TM) oblique incidence and loop currents for transverse electric (TE) oblique incidence. Moreover, the presence of the pin creates an additional current that we assume to be constant on the pin and radial on the patches. An auxiliary cylindrical structure is used to accurately model this current.

Received 19 July 2024; revised 18 December 2024; accepted 23 December 2024. Date of publication 20 January 2025; date of current version 7 May 2025. This work was supported in part by the European Space Agency (ESA) for the Project "Antenna User Terminal with Wide Angle Impedance Matching Metamaterial Radome" under Contract 4000127381/19/NL/AF. *(Corresponding author: Alexander J. van Katwijk.)*

The authors are with the Microelectronics Department of the EEMCS Faculty, Delft University of Technology, 2628 CD Delft, The Netherlands (e-mail: a.j.vankatwijk@tudelft.nl; a.neto@tudelft.nl; d.cavallo@tudelft.nl).

Digital Object Identifier 10.1109/TAP.2025.3529189

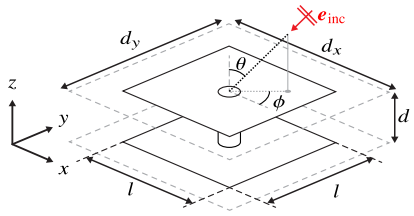

Fig. 2. Geometry of the pin-patch structure with geometrical parameters. The incident field $\boldsymbol{e}_{\text{inc}}$ is a plane wave with incidence angles θ and ϕ.

To validate the method, we study the scattering for TE and TM plane-wave incidence from all directions. The selected basis functions systematically yield a good estimation of the reflection and transmission coefficients, agreeing well with the results from a commercial full-wave solver.

II. Spectral-Domain MoM for Hybrid ADLs

The proposed analysis method uses a spectral-domain MoM to model the currents that are excited on the structure by the incident plane wave. The structure under investigation is illustrated in Fig. 2 and consists of two metal patches connected by a vertical pin, periodic along x and y with periods d_x and d_y, respectively, in free space. The structure is assumed to be smaller than a quarter wavelength so that it is well below resonance. The two patches are centered at $x = y = 0$ and $z = \pm d/2$ and are assumed to be square with sides l and infinitesimally thin in z. The pin is taken as circular with radius r_1 and height d, centered in the origin. A plane wave incident from the angles θ and ϕ with wave number k_0 is considered.

To find the currents on the structure, an electric field integral equation is set up based on the requirement that the tangential electric field vanishes on the metal. This means that the scattered field, given by the convolution of the currents on the structure with Green's function, must be equal and opposite to the incident field

$$-\int_{-\infty}^{\infty}\int_{-\infty}^{\infty}\int_{-\infty}^{\infty}\bar{\bar{\boldsymbol{g}}}(\boldsymbol{r},\boldsymbol{r}')\boldsymbol{j}(\boldsymbol{r})d\boldsymbol{r}' = \boldsymbol{e}_{\text{inc}}(\boldsymbol{r}) \tag{1}$$

where $\bar{\bar{\boldsymbol{g}}}$ is the dyadic Green's function and $\boldsymbol{j}$ are the equivalent currents on the structure. The equivalent currents are expanded into a set of N basis functions, periodic in x and y

$$\boldsymbol{j}(\boldsymbol{r}) = \sum_{n_x=-\infty}^{\infty}\sum_{n_y=-\infty}^{\infty}\sum_{n=1}^{N} i_n \boldsymbol{b}_n(x-n_x d_x, y-n_y d_y, z) \cdot e^{-jk_{x0}n_x d_x} e^{-jk_{y0}n_y d_y} \tag{2}$$

where i_n is the unknown complex amplitude of the nth basis function $\boldsymbol{b}_n$. The exponential terms account for the phase shifts in the unit cell with indices n_x and n_y, due to the oblique plane-wave incidence. These are related to the x, y components of the propagation vector $\boldsymbol{k}_0 = (k_{x0}, k_{y0}, k_{z0})$, where $k_{x0} = k\sin\theta\cos\phi$, $k_{y0} = k\sin\theta\sin\phi$, $k_{z0} = k\cos\theta$, and k is the free-space wavenumber.

The incident field $\boldsymbol{e}_{\text{inc}}(\boldsymbol{r})$ is a generic plane wave traveling in the $-z$-direction, which can be expressed as the superposition of TM and TE components

$$\boldsymbol{e}_{\text{inc}}(\boldsymbol{r}) = (V_{\text{TM}}\hat{\theta} + V_{\text{TE}}\hat{\phi})e^{-jk_{x0}x}e^{-jk_{y0}y}e^{+jk_{z0}z}. \tag{3}$$

According to the Galerkin projection method, the test functions are chosen to be equal to the basis functions. By applying the spectral-domain method and the Floquet theorem, we find the mutual impedances for Cartesian basis functions as

$$Z_{n'n} = -\frac{1}{2\pi}\frac{1}{d_x d_y}\sum_{m_x=-\infty}^{\infty}\sum_{m_y=-\infty}^{\infty}\int_{-\infty}^{\infty}\bar{\bar{\boldsymbol{G}}}(\boldsymbol{k}_m)\boldsymbol{B}_n(\boldsymbol{k}_m) \cdot \boldsymbol{B}_{n'}(-\boldsymbol{k}_m)dk_z \tag{4}$$

where $\boldsymbol{k}_m = (k_{xm}, k_{ym}, k_z)$, $k_{xm} = k_{x0} - 2\pi m_x/d_x$, and $k_{ym} = k_{y0} - 2\pi m_x/d_y$ are the Floquet wavenumbers, and $\bar{\bar{\boldsymbol{G}}}$ is the spectral free-space dyadic Green's function. $\boldsymbol{B}_n$ and $\boldsymbol{B}_{n'}$ are the three-dimensional Fourier transforms of the basis functions. For all expressions used in this work, the integral in k_z can be evaluated in closed form using the residue theorem [16]. Since the basis functions are also chosen such that their relevant transforms are known in closed form, the computation of the mutual impedance matrix is purely analytical.

Using the mutual impedance matrix, the unknown current weights $\boldsymbol{i}$ can be found as

$$\boldsymbol{i} = \boldsymbol{Z}^{-1}\boldsymbol{v}_{\text{inc}} \tag{5}$$

where the mutual impedance matrix $\boldsymbol{Z}$ for the basis functions is given by (4). The incident voltage on the n'th basis function is given by the projection of the incident field onto the test function

$$v_{\text{inc},n'} = \boldsymbol{B}_{n'}(-k_{x0}, -k_{y0}, +k_{z0}) \cdot [(V_{\text{TM}}\cos\theta\cos\phi - V_{\text{TE}}\sin\phi)\hat{x} + (V_{\text{TM}}\cos\theta\sin\phi + V_{\text{TE}}\cos\phi)\hat{y} + (-V_{\text{TM}}\sin\theta)\hat{z}]. \tag{6}$$

The basis functions can be freely chosen and a common choice is small-domain basis functions such as Rao–Wilton–Glisson [17]. However, to enable efficient evaluation of the matrix inversion, the number of basis functions should be minimized. In this work, 9 entire domain basis functions are chosen that accurately model the shape of the currents excited on the structure.

A. Scattering Parameters

The scattered field can be found in the fundamental Floquet mode as

$$\boldsymbol{e}_{\text{scat}}(x,y,z) = \frac{1}{d_x d_y}\sum_{n=1}^{N} i_n \frac{1}{2\pi}\int_{-\infty}^{\infty}\bar{\bar{\boldsymbol{G}}}(k_{x0}, k_{y0}, k_z) \cdot \boldsymbol{B}_n(k_{x0}, k_{y0}, k_z)dk_z. \tag{7}$$

The scattering parameters for TE and TM plane waves are given by

$$\Gamma_{\text{TM}} = \frac{e_{\text{scat,TM}}}{e_{\text{inc,TM}}}, \quad \Gamma_{\text{TE}} = \frac{e_{\text{scat,TE}}}{e_{\text{inc,TE}}} \tag{8}$$

where the TM and TE components of the field are related to the Cartesian components by

$$e_{\text{TM}} = e_x\cos\phi + e_y\sin\phi \tag{9}$$

$$e_{\text{TE}} = -e_x\sin\phi + e_y\cos\phi. \tag{10}$$

It should be pointed out that the method presented here is limited to free space, but it could be extended to include dielectric slabs by considering the layered media Green's function in the spectral domain, with a procedure similar to [18].

III. Entire-Domain Basis Functions

We assume that an incident plane wave can give rise to three currents on the patches, which are illustrated in Fig. 3, which are referred to as linear, loop, and radial. The currents are assumed to be variable separable in either Cartesian or cylindrical coordinates. Since the patches are assumed to be infinitesimally thin, the current distribution along z for all basis functions on the patches is given by $b_z(z) = \delta(z)$, where $\delta(z)$ is the Dirac delta function.

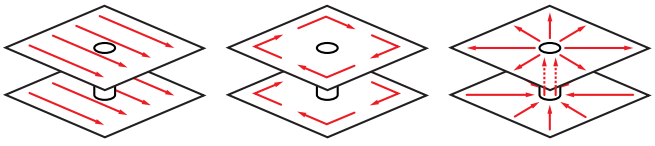

(a) (b) (c)

Fig. 3. Shapes of the currents that are excited on the structure. (a) Linear current. (b) Loop current. (c) Radial current.

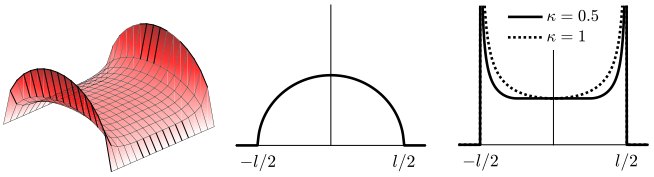

(a) (b) (c)

Fig. 4. Basis functions used to model the linear currents on the pin-patch ADL. (a) Three-dimensional visualization of the shape of the basis function along $\hat{x}$. (b) Inverse edge singular distribution. (c) Adjustable edge singular distribution.

A. Linear Current

The first type of basis function describes the dominant current contribution under normal incidence, which is linearly polarized, as illustrated in Fig. 3(a). The direction of this linear current depends on the azimuth and polarization of the incident field. The component of this current along $\hat{x}$ is modeled with an inverse edge singular distribution along x and an adjustable edge singular distribution along y. The adjustable edge singular [19] is chosen to more accurately model the flattening of the current due to the capacitive effect between neighboring patches. A 3-D visualization of the shape of the linear basis function along $\hat{x}$ is shown in Fig. 4(a).

The inverse edge singular distribution [Fig. 4(b)] is given by

$$e(u) = \frac{4}{\pi l}\sqrt{1-\left(\frac{2u}{l}\right)^2}\,\mathrm{rect}\left(\frac{u}{l}\right) \tag{11}$$

where u is either x or y, l is the length of the function, and the factor $4/(\pi l)$ is used to normalize the integral of the distribution to 1. Here, rect is the unit rectangular function, that is, $\mathrm{rect}(u) = 1$ when $|u| \leq 0.5$ and 0 otherwise.

The adjustable edge singular distribution [Fig. 4(c)] is given by

$$a_\kappa(u) = \frac{\mathrm{rect}\left(\frac{2u+l}{l\kappa} - \frac{1}{2}\right)}{\sqrt{1-\left(\frac{2u+l}{\kappa l} - 1\right)^2}} + \frac{\mathrm{rect}\left(\frac{2u-l}{l\kappa} + \frac{1}{2}\right)}{\sqrt{1-\left(\frac{2u-l}{\kappa l} + 1\right)^2}} + \mathrm{rect}\left(\frac{u}{l(1-\kappa)}\right)\mathrm{sign}(1-\kappa) \tag{12}$$

where

$$\mathrm{sign}(x) = \begin{cases} -1, & \text{if } x < 0 \\ 0, & \text{if } x = 0 \\ 1, & \text{if } x > 0. \end{cases} \tag{13}$$

The parameter κ defines the fraction of the function that is edge singular and was found using a full-wave solver to be linear with the ratio of the patch size and the periodicity. A linear fit of the values of κ that best describe the current on the patch yields $\kappa = 1.226$–$1.1489\, l/d$, where l and d are the lengths and the period of the function.

The linear basis functions along $\hat{x}$ can be written as

$$\boldsymbol{b}_{\mathrm{linear},\hat{x}}(x, y, z) = e(x - x_n)a_\kappa(y - y_n)\delta(z - z_n)\hat{x} \tag{14}$$

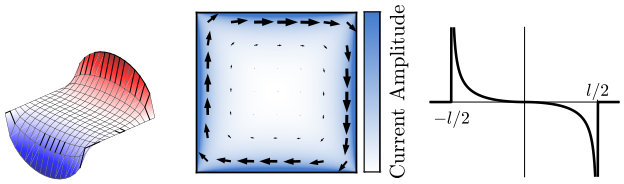

(a) (b) (c)

Fig. 5. Basis functions used to model the linear currents on the pin-patch ADL. (a) Three-dimensional visualization of the shape of the basis function along $\hat{x}$. (b) Color map of current amplitude when the two basis functions have equal weight, with arrows denoting the direction of the current. (c) Odd edge singular distribution.

where $\boldsymbol{r}_n = (x_n, y_n, z_n)$ is the center of the nth basis function. The linear basis function along $\hat{y}$ is the same, with x and y swapped in the expression. The linear currents on the patches also give rise to vertical currents on the pin. However, the currents on either side of the pins are equal and opposite, so they do not contribute to scattering for pin radii that are much smaller than the wavelength. As such, these currents can be neglected in the analysis.

Since the basis functions are to be used in a spectral-domain MoM, the Fourier transforms of the functions are determined in closed form to reduce the computational complexity. The Fourier transform of an inverse edge singular distribution is given by

$$E(k) = \frac{4}{\pi l}\frac{\pi}{k}J_1\left(k\frac{l}{2}\right) \tag{15}$$

where J_ν is the νth-order Bessel function of the first kind. The Fourier transform of the adjustable edge singular distribution of length l is

$$A_\kappa(k) = l\kappa\frac{\pi}{2}\left[J_0\left(k\frac{l}{2}\kappa\right)\cos\left(k\frac{l}{2}(1-\kappa)\right) - \mathbf{H}_0\left(k\frac{l}{2}\kappa\right)\sin\left(k\frac{l}{2}(1-\kappa)\right)\right] + l(1-\kappa)\,\mathrm{sinc}\left(k\frac{l}{2}(1-\kappa)\right) \tag{16}$$

where $\mathbf{H}_\alpha$ is the αth-order Struve function of the first kind. Hence, the spectral-domain linear basis functions can be written as

$$\boldsymbol{B}_{\mathrm{linear},\hat{x}}(\boldsymbol{k}) = E(k_x)A_\kappa(k_y)e^{j\boldsymbol{k}\boldsymbol{r}_n}\hat{x} \tag{17}$$

where $\boldsymbol{k} = (k_x, k_y, k_z)$.

B. Loop Current

For grazing TE incidence, a loop current is excited on the patches, as illustrated in Fig. 3(b). This loop current can be modeled using another pair of basis functions along $\hat{x}$ and $\hat{y}$ on each patch. For example, the current along $\hat{x}$ is modeled using an inverse edge singular along x, and an odd edge singular along y. A 3-D visualization of the shape of the basis function along $\hat{x}$ is shown in Fig. 5(a). The loop is formed by the superposition of the two basis functions, and an example of when their amplitudes are equal is shown in Fig. 5(b).

The odd edge singular distribution [Fig. 5(c)] is given by

$$o(u) = \left(\frac{1}{\sqrt{1-\left(\frac{2u}{l}\right)^2}} - 1\right)\left[\mathrm{rect}\left(\frac{2u}{l} + \frac{1}{2}\right) - \mathrm{rect}\left(\frac{2u}{l} - \frac{1}{2}\right)\right] \tag{18}$$

with Fourier transform

$$O(k) = e^{jkl/2}[J_0(kl) - j\mathbf{H}_0(kl)] - e^{-jkl/2} \cdot [J_0(-kl) - j\mathbf{H}_0(-kl)]. \tag{19}$$

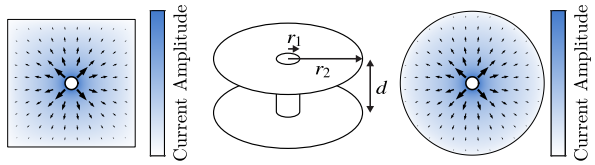

Fig. 6. Current amplitude due to the radial spreading on the (a) square and (b) round patch, with arrows denoting the direction of the current. (c) Equivalent circular geometry used to model the current on the pin and the radial current on the patches.

The $\hat{x}$-oriented component of the loop basis function is given by

$$\boldsymbol{b}_{\text{loop},\hat{x}}(x-x_n, y-y_n, z-z_n) = e(x-x_n)o(y-y_n)\delta(z-z_n)\hat{x}. \tag{20}$$

The component along $\hat{y}$ is the same, with x and y swapped in the expression. The loop current has a null in the center, so no current is excited on the pin. The spectral-domain loop basis function is

$$\boldsymbol{B}_{\text{loop},\hat{x}}(\boldsymbol{k}) = E(k_x)O(k_y)e^{j\boldsymbol{k}\boldsymbol{r}_n}\hat{x}. \tag{21}$$

C. Currents Due to the Pin

The vertical component of the field interacts with the pin and generates a current on the pin itself. This vertical current terminates in the patches and spreads radially across the patches [see Fig. 6(a)]. The radial spreading can be described using the distribution

$$\frac{1}{\sqrt{x^2+y^2}}\,\text{rect}\left(\frac{x}{l}\right)\text{rect}\left(\frac{y}{l}\right). \tag{22}$$

This function has a discontinuity at the edge of the patch, so it is multiplied by the inverse edge singular function to force it to zero at the edges of the patch, resulting in

$$\frac{1}{\sqrt{x^2+y^2}}\,\text{rect}\left(\frac{x}{l}\right)\text{rect}\left(\frac{y}{l}\right)\sqrt{1-\left(\frac{2x}{l}\right)^2}\sqrt{1-\left(\frac{2y}{l}\right)^2}. \tag{23}$$

However, the Fourier transform of (23) is not known in closed form and would, therefore, require a computationally expensive numerical evaluation. Since the current is along the radial direction, it is convenient to instead model it using cylindrical coordinates. This means that the pin and patches are modeled using an auxiliary circular structure, as shown in Fig. 6(b). The radial current is modeled with the product of $1/\rho$ and an inverse edge singular function, where $1/\rho$ models the radial spreading of the current, and the inverse edge singular function ensures that the current goes to zero at the edge of the patch. The current is assumed to be constant in azimuth ϕ. The resulting current on a circular patch is shown in Fig. 6(c).

The radial current on the patch inside the radius of the pin ($0 < \rho < r_1$) is zero due to symmetry, so the basis function must be set to zero for $\rho < r_1$. To retain the closed-form Hankel transforms, this zero was introduced by subtracting a second-order Taylor expansion in $\rho = 0$ of the distribution. The basis function is shown in Fig. 7(a) and can be written as

$$\begin{aligned}\boldsymbol{b}_{\text{radial}}(\rho, z) &= \left[\frac{1}{\rho}\sqrt{1-\left(\frac{\rho}{r_2}\right)^2}\,\text{rect}\left(\frac{\rho}{2r_2}\right) - \left(1-\frac{\rho^2}{2r_2^2}\right)\text{rect}\left(\frac{\rho}{2r_1}\right)\right] \\ &\quad\cdot\delta(z-z_n)\hat{\rho}\end{aligned} \tag{24}$$

where r_2 is the radius of the equivalent circular patch. The value of this radius is chosen such that the area of the circle matches that of the patch, so $r_2 = l/\sqrt{\pi}$. To show the validity of this approach, a pin-patch structure is placed in a periodic environment and illuminated

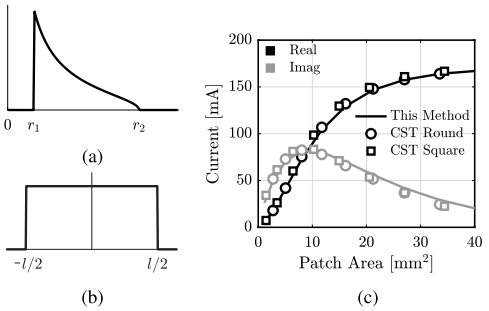

Fig. 7. (a) Radial current distribution and (b) rectangular distribution. (c) Vertical current on the pin of the pin-patch structure versus patch area under TM plane-wave illumination incident at a grazing angle (89°).

with a TM-polarized incident plane wave incident at a grazing angle ($\theta = 89°$). The structure consists of two circular patches of radius $r_2 = 1$ mm or two square patches of length $l_x = l_y = 1.77$ mm. The patches are spaced $d = 0.2$ mm apart and placed in a periodic lattice of $d_x = d_y = 2.5$ mm. Fig. 7(c) shows the currents on the pin as a function of patch area for square and circular patches, which are seen to be in close agreement with results obtained using the frequency-domain solver of CST Microwave Studio 2022 [20].

The vertical current on the pin is assumed to be only on the surface of the pin (infinitesimal in ρ) and to be constant in z and ϕ [see Fig. 7(b)]. The current is oriented along $\hat{z}$ and is given by

$$\boldsymbol{b}_{\text{pin}}(\rho, z) = \delta(\rho - r_1)\,\text{rect}\left(\frac{z-z_n}{d}\right)\hat{z}. \tag{25}$$

The basis functions defined in (24) and (25) are discontinuous. To ensure continuity of the current at the junctions between the pin and the patches, the amplitude of these basis functions is set to be equal. This is done by summing the rows and columns of the impedance matrix corresponding to these basis functions. Additionally, due to symmetry, the current on the pin and the radial current on the patches do not couple to the linear and loop currents and the mutual impedances between them are zero for any incident plane wave.

To calculate the mutual and self-impedances of the three cylindrical basis functions in the rectangular periodic lattice, a spectral-domain MoM was developed that accepts basis functions in Cartesian or cylindrical coordinates. The expressions for the mutual impedances and incident voltages of cylindrical basis functions are given in the Appendix and involve Hankel transforms of the basis functions. For this reason, the Hankel transforms of 0th and first order are shown below instead of the Fourier transforms that were shown for the Cartesian basis functions.

The Hankel transforms of the 0th and first order of a function $f(\rho)$ are denoted by

$$F_{J_\nu}(k_\rho) = \int_0^\infty f(\rho)J_\nu(k_\rho\rho)\rho d\rho \tag{26}$$

where ν is 0 or 1. In the cylindrical MoM expression, the Hankel transform is applied to the ρ-dependence, and the Fourier transform is used for the z-dependence. The resulting transforms of the radial basis function are given by

$$\begin{aligned}\boldsymbol{B}_{\text{radial},J_0}(k_\rho, k_z) &= \left[-\frac{r_1}{2}J_0(k_\rho r_1)(2-\pi\mathbf{H}_1(k_\rho r_1)\left(1+\frac{1}{2k_\rho^2 r_2^2}\right)\right. \\ &\quad + \frac{r_1}{2}J_1(k_\rho r_1)(k_\rho\frac{r_1}{r_2^2} - \pi\mathbf{H}_0(k_\rho r_1)\left(1+\frac{1}{2k_\rho^2 r_2^2}\right) \\ &\quad \left. + \frac{r_2}{4}\pi\left(J_0\left(k_\rho\frac{r_2}{2}\right)^2 + J_1\left(k_\rho\frac{r_2}{2}\right)^2\right)\right]e^{j\boldsymbol{k}\boldsymbol{r}_n}\hat{\rho}\end{aligned} \tag{27}$$

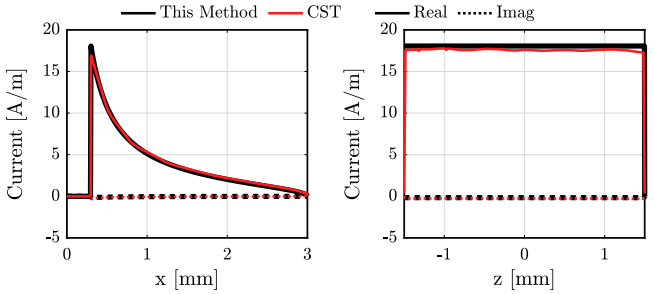

Fig. 8. Current on a circular pin-patch structure under TM plane-wave illumination, incident at $\theta = 89°$. (a) Current along x on the top patch. (b) Current along z on the pin.

$$\boldsymbol{B}_{\text{radial},J_1}(k_\rho, k_z) = \frac{1}{k_\rho}\left[J_0(k_\rho r_1) + \frac{r_1^2}{2r_2^2}J_2(k_\rho r_1) - \text{sinc}(k_\rho r_2)\right] e^{j\boldsymbol{k}\boldsymbol{r}_n}\hat{\rho}. \quad (28)$$

For the basis function that models the currents on the pin, the transforms are given by

$$\boldsymbol{B}_{\text{pin},J_v}(k_\rho, k_z) = \frac{1}{2\pi}J_v(k_\rho r_1) l \,\text{sinc}\left(k_z\frac{l}{2}\right) e^{j\boldsymbol{k}\boldsymbol{r}_n}\hat{z}. \quad (29)$$

It can be noted that, while the linear and loop basis functions would also be suitable for rectangular patches ($l_x \neq l_y$) and rectangular unit cells ($d_x \neq d_y$), the introduced radial current is only valid in the specific case of square patches with the pin centered in the patch. Such a hypothesis is made to simplify the problem, since the square patch is approximated as a circle to find the amplitude of the current on the pin, and the loop and linear currents do not couple with the pin by symmetry only if the pin is centered.

IV. Validation

The method is validated by comparing the results with the commercial full-wave solver CST Microwave Studio. To verify the accuracy of the circular pin-patch analysis, the circular pin-patch structure in Fig. 7(c) is again considered with a 30-GHz TM-polarized plane wave incident at an elevation angle of 89°. The currents on the patches and the pin are shown in Fig. 8(a) and (b), respectively. It is seen that the method can accurately model the shape, amplitude, and phase of the current on the circular patches and the pin.

As a further example, the square pin-patch structure used in [5] is analyzed. This consists of two square patches with sides $l = 1.09$ mm separated by a distance $d = 0.254$ mm. The two patches are connected by a pin with radius $r_1 = 0.1$ mm and height d. The structure is in a periodic environment along x and y with a periodicity of $d_x = d_y = 1.45$ mm. The structure is illuminated by a 30-GHz TE- or TM-polarized plane wave incident at an angle $\theta = 10°$ along the $\phi = 0°$ plane. The currents on the top patch are shown on cuts along x and y in Fig. 9(a) and (b), respectively. A good agreement of our method with CST can be seen for most of the cut, but an increasing difference is seen near the pin. This difference is due to the current entering and exiting the pin, which was neglected for the linear current, but causes a crowding effect near the edge of the pin. To show this effect, the current on the patch is extracted from CST and the path of the currents is traced. A closeup of the region around the pin is shown in Fig. 9(c), where the crowding effect is clearly visible. This crowding is a local effect and does not influence the scattering of the structure, as will be shown by the scattering parameters.

The currents can be used to calculate the scattered field and scattering parameters using the expressions in Section II-A. The structure

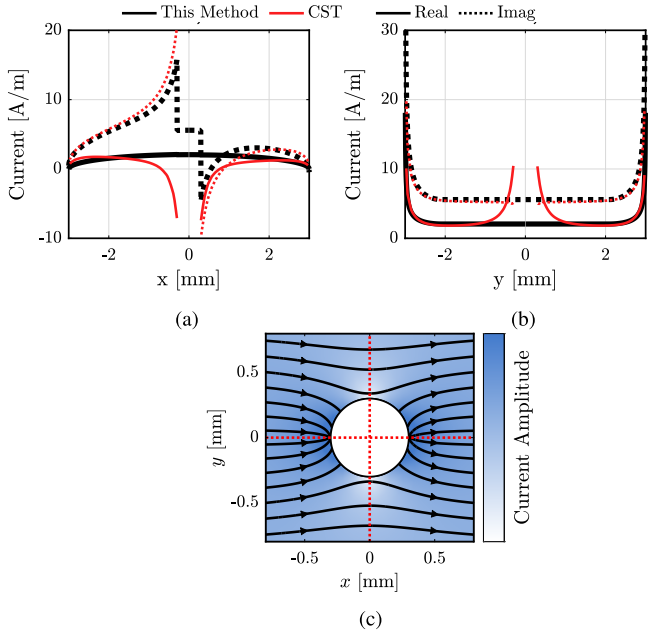

Fig. 9. Current on a circular pin-patch structure under TM plane-wave incidence from $\theta = 10°$. (a) $\hat{x}$-oriented current on the top patch versus x and (b) versus y. (c) Closeup of the real part of the current near the pin on the top patch (the two cuts of (a) and (b) are shown in red).

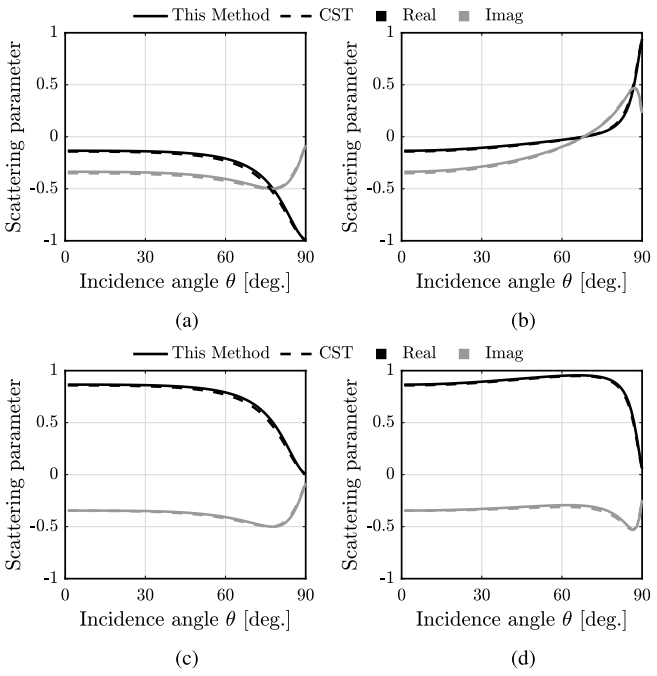

Fig. 10. Scattering parameters at 30 GHz vs incidence angle for plane wave incidence on the pin-patch structure used in [5]. (a) Reflection under TE and (b) TM incidence, and (c) transmission under TE and (d) TM incidence.

for which the currents were shown in Fig. 9 is analyzed, and the scattering parameters are computed for the varying angle of incidence θ in the plane $\phi = 0°$. The resulting reflection coefficients are shown in Fig. 10 to be in good agreement with CST. A similar agreement was observed for plane-wave incidence in other azimuthal planes.

The results shown in Fig. 10 took 8 s for 90 scanning angles using the proposed method, and 40 min in CST. When optimizing a design, a single incidence angle is generally considered, and the geometrical parameters are changed for each iteration. Evaluating a single angle took 90 msec using the proposed method, and 4 min in CST. This means that the method can provide the computational efficiency that

is required when optimizing a design and enable the use of simple iterative techniques to design a particular behavior.

V. Conclusion

A unit cell consisting of a set of two patches connected by a vertical pin was analyzed. Such a periodic structure was shown to significantly reduce the X-pol in wideband arrays that use artificial dielectrics in their superstrate. An analysis technique is proposed based on the spectral-domain MoM. The key aspect of the procedure is the use of entire-domain basis functions to define the electric current distribution on the structure.

Three groups of basis functions are defined and shown to describe accurately the currents. Currents and reflection coefficients obtained with the proposed method are shown to be in good agreement with those obtained in a commercial full-wave solver. The method can speed up the analysis of the structure by a factor of 2500 with respect to CST for a single incidence angle and frequency. This can be beneficial for the design of ADL superstrates for antennas or arrays, to improve polarization purity.

Appendix

The expressions below give the mutual impedance for any pair of basis functions in cylindrical coordinates, in an infinitely periodic environment along x and y. These expressions differ depending on the orientation of the basis and test functions. It is assumed that all basis functions are constant in ϕ and separable in ρ and z, that is,

$$\boldsymbol{b}(\rho,\phi,z) = b_\rho(\rho)b_z(z)\hat{b} \tag{30}$$

thus the Fourier/Hankel transforms are only functions of k_ρ and k_z

$$\boldsymbol{B}(k_\rho,k_z) = B_{\rho,J_v}(k_\rho)B_Z(k_z)\hat{b}. \tag{31}$$

When both basis and test functions are along ρ ($\hat{b}_n = \hat{b}_{n'} = \hat{\rho}$), the mutual impedance can be found using

$$Z_{n'n,\rho\rho} = +\frac{2\pi}{d_x d_y}\sum_{m_x}\sum_{m_y}\int_{-\infty}^{\infty}\boldsymbol{G}(k_{xm},k_{ym},k_z)B_{n\rho,J_1}(k_{\rho m}) \cdot B_{n'\rho,J_1}(k_{\rho m})(\hat{x}\cos\alpha_m+\hat{y}\sin\alpha_m)^2 B_{nz}(k_z)B_{n'z}(k_z)dk_z \tag{32}$$

where $\alpha_m = \arctan(k_{ym}/k_{xm})$ and $k_{\rho m} = \sqrt{k_{xm}^2+k_{ym}^2}$.

When $\hat{b}_n = \hat{\rho}$ and $\hat{b}_{n'} = \hat{z}$

$$Z_{n'n,\rho z} = -\frac{2\pi}{d_x d_y}\sum_{m_x}\sum_{m_y}\int_{-\infty}^{\infty}\boldsymbol{G}(k_{xm},k_{ym},k_z)B_{n\rho,J_1}(k_{\rho m}) \cdot B_{n'\rho,J_0}(k_{\rho m})\,j(\hat{x}\cos\alpha_m+\hat{y}\sin\alpha_m)\hat{z}B_{nz}(k_z)B_{n'z}(k_z)dk_z. \tag{33}$$

When $\hat{b}_n = \hat{b}_{n'} = \hat{z}$

$$Z_{n'n,zz} = -\frac{2\pi}{d_x d_y}\sum_{m_x}\sum_{m_y}\int_{-\infty}^{\infty}\boldsymbol{G}(k_{xm},k_{ym},k_z)B_{n\rho,J_0}(k_{\rho m}) \cdot B_{n'\rho,J_0}(k_{\rho m})\hat{z}\hat{z}B_{nz}(k_z)B_{n'z}(k_z)dk_z. \tag{34}$$

For a cylindrical test function along $\hat{\rho}$, the incident voltage is

$$v_{\text{inc},n'} = \left[(V_{\text{TM}}\cos\theta\cos\phi - V_{\text{TE}}\sin\phi)\cos\alpha_0 + (V_{\text{TM}}\cos\theta\sin\phi + V_{\text{TE}}\cos\phi)\sin\alpha_0\right] \cdot 2\pi j\,B_{n'\rho,J_1}(-k_{\rho 0})B_{n'z}(-k_{z0}) \tag{35}$$

and, for a cylindrical test function along $\hat{z}$

$$v_{\text{inc},n'} = -V_{\text{TM}}\sin\theta\,2\pi\,B_{n'\rho,J_0}(-k_{\rho 0})B_{n'z}(+k_{z0}). \tag{36}$$

References

[1] D. H. Schaubert, J. Shin, and G. Wunsch, "Characteristics of single-polarized phased array of tapered slot antennas," in *Proc. Int. Symp. Phased Array Syst. Technol.*, Boston, MA, USA, 1996, pp. 102–106.

[2] R. Kindt and D. Taylor, "Polarization correction in dual-polarized phased arrays of flared notches," in *Proc. IEEE Int. Symp. Antennas Propag. (APSURSI)*, Spokane, WA, USA, Jul. 2011, pp. 1961–1964.

[3] R. Ozzola, A. Neto, U. Imberg, and D. Cavallo, "Connected slot array with interchangeable ADL radome for sub-8 GHz 5G applications," *IEEE Trans. Antennas Propag.*, vol. 72, no. 1, pp. 992–997, Jan. 2024.

[4] D. Cavallo and R. M. van Schelven, "Closed-form analysis of artificial dielectric layers with non-periodic characteristics," in *Proc. 13th Eur. Conf. Antennas Propag. (EuCAP)*, Krakow, Poland, Mar. 2019, pp. 1–5.

[5] A. J. van Katwijk, C. M. C. Martin, G. Toso, and D. Cavallo, "On the cross-polarization levels of arrays with wide angle impedance matching layers," *IEEE Trans. Antennas Propag.*, vol. 72, no. 6, pp. 5078–5087, Jun. 2024.

[6] D. Sievenpiper, L. Zhang, R. F. J. Broas, N. G. Alexopolous, and E. Yablonovitch, "High-impedance electromagnetic surfaces with a forbidden frequency band," *IEEE Trans. Microw. Theory Techn.*, vol. 47, no. 11, pp. 2059–2074, Nov. 1999.

[7] A. J. V. Katwijk, A. Neto, G. Toso, and D. Cavallo, "Design of wideband wide-scanning dual-polarized phased array covering simultaneously both the Ku- and the Ka-Satcom bands," in *Proc. 14th Eur. Conf. Antennas Propag. (EuCAP)*, Copenhagen, Denmark, Mar. 2020, pp. 1–3.

[8] A. B. Yakovlev, M. G. Silveirinha, O. Luukkonen, C. R. Simovski, I. S. Nefedov, and S. A. Tretyakov, "Characterization of surface-wave and leaky-wave propagation on wire-medium slabs and mushroom structures based on local and nonlocal homogenization models," *IEEE Trans. Microw. Theory Techn.*, vol. 57, no. 11, pp. 2700–2714, Nov. 2009.

[9] R. Mittra, C. H. Chan, and T. Cwik, "Techniques for analyzing frequency selective surfaces—A review," *Proc. IEEE*, vol. 76, no. 12, pp. 1593–1615, Dec. 1988.

[10] D. B. Davidson and J. T. Aberle, "An introduction to spectral domain method-ofmmoments formulations," *IEEE Antennas Propag. Mag.*, vol. 46, no. 3, pp. 11–19, Jun. 2004.

[11] J. Wang, S. J. Wang, J. Li, J. Liu, L.-Y. Xiao, and Q. H. Liu, "Spectral-element spectral-integral (SESI) method for doubly periodic problems with 3-D scatterers embedded in multiple regions of layered media," *IEEE Trans. Microw. Theory Techn.*, vol. 71, no. 3, pp. 977–987, Mar. 2023.

[12] V. Volski and G. A. E. Vandenbosch, "Quasi 3-D mixed potential integral equation formulation for periodic structures," *IEEE Trans. Antennas Propag.*, vol. 61, no. 4, pp. 2068–2076, Apr. 2013.

[13] I. Stevanovic, P. Crespo-Valero, K. Blagovic, F. Bongard, and J. R. Mosig, "Integral-equation analysis of 3-D metallic objects arranged in 2-D lattices using the Ewald transformation," *IEEE Trans. Microw. Theory Techn.*, vol. 54, no. 10, pp. 3688–3697, Oct. 2006.

[14] M. Lucido, "A new high-efficient spectral-domain analysis of single and multiple coupled microstrip lines in planarly layered media," *IEEE Trans. Microw. Theory Techn.*, vol. 60, no. 7, pp. 2025–2034, Jul. 2012.

[15] S. C. Pavone, M. Faenzi, E. Martini, M. Albani, and S. Maci, "Closed form basis function Fourier spectra for dispersion calculation of metasurfaces made by circular and elliptical ring patches," in *Proc. 12th Eur. Conf. Antennas Propag. (EuCAP)*, Apr. 2018, pp. 1–3.

[16] A. J. van Katwijk, "Analysis and design of wideband phased arrays for Ku- and Ka-band Satcom applications," Dept. Microelectron., Delft Univ. Technol., Delft, The Netherlands, Tech. Rep., 2024.

[17] S. Rao, D. Wilton, and A. Glisson, "Electromagnetic scattering by surfaces of arbitrary shape," *IEEE Trans. Antennas Propag.*, vol. AP-30, no. 3, pp. 409–418, May 1982.

[18] H. T. Shivamurthy, "On the design and analysis of micro-metric resolution arrays in integrated technology for near-field dielectric spectroscopy," Ph.D. dissertation, Dept. Microelectron., Delft Univ. Technol., Delft, The Netherlands, 2020.

[19] R. O. Ribeiro, M. V. T. Heckler, and A. F. Tinoco, "Entire domain basis function with accurate edge condition for rectangular microstrip antennas," *IEEE Antennas Wireless Propag. Lett.*, vol. 18, pp. 123–127, 2019.

[20] Dassault Systèmes. *CST Studio Suite*. Accessed: May 27, 2024. [Online]. Available: https://www.3ds.com/products/simulia/cst-studio-suite